# Modeling hydrodynamics and heat exchange in response to liquid metal buoyant flow in a rectangular channel in a coplanar magnetic field



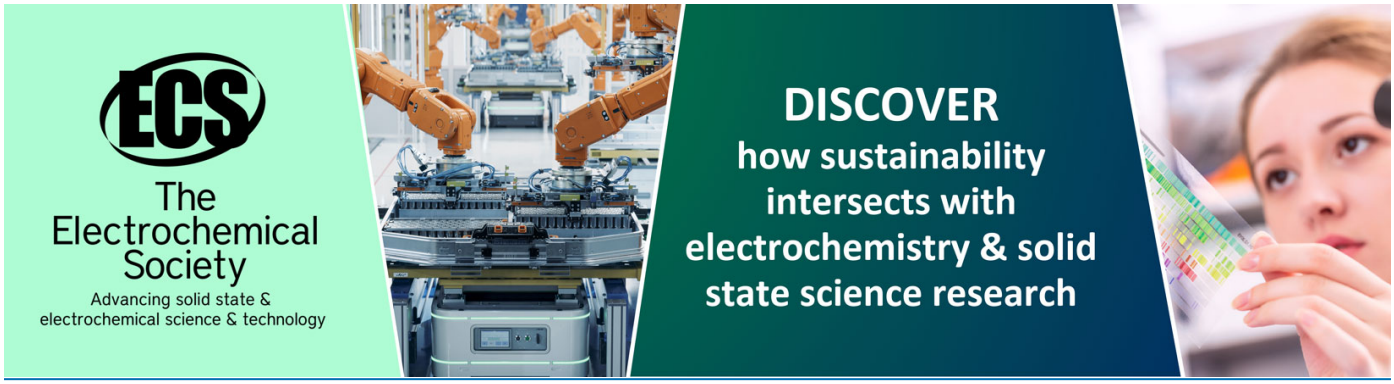

IOP Conf. Series: Journal of Physics: Conf. Series **1133** (2018) 012021 doi:10.1088/1742-6596/1133/1/012021

# Modeling hydrodynamics and heat exchange in response to liquid metal buoyant flow in a rectangular channel in a coplanar magnetic field

**P V Kostychev[1], N Yu Pyatnitskaya[1,2], N G Razuvanov[1,2], P A Sardov[2] and E V Sviridov[1,2]**

[1] National Research University «MPEI», Moscow, Russia
[2] Joint Institute for High Temperatures of RAS, Moscow, Russia

E-mail: nikita.razuvanov@mail.ru

**Abstract.** The hydrodynamics and heat exchange in response to liquid metal (LM) buoyant flow in a rectangular channel with approximately 3/1 aspect ratio in a coplanar magnetic field (MF) on the assumption of one-sided channel heating have been studied. The flow configuration is approximated to the heat exchange channel of the cooling system of a TOKAMAK fusion reactor LM blanket. Experiments were performed on the mercury magneto-hydrodynamic (MHD) test stand as part of MPEI – JIHT of RAS facility. Under the conditions of buoyant flow, the measurable effect of thermal gravitational convection (TGC) interacting with the external MF in some environments was detected, it causes occurrence and development of layered flow variabilities. Averaged velocity, channel wall temperature profiles are shown. The MF causes suppression of turbulent transfer resulting in an increase in heated wall temperature. A numerical model of target values under experimental conditions is proposed. In the process of numerical simulation, the differential equation system: the continuity equation, the motion equation for three velocity components and the energy equation, was solved. To compute turbulence, the Reihardt model adapted for the rectangular channel was used. Computational data agree satisfactorily with experimental data.

## 1. Introduction

In recent years, Russia has been heavily developing hybrid fusion plants – the fusion neutron source (FNS) [1] – as nuclear industry development alternative. These 14-MeV sources are planned to be used for post-combustion of long-lived actinides and fuel production for the traditional nuclear power industry. The hybrid reactor will mainly utilize liquid metals (LM) as the heat transfer medium. At present, the sole project with the closest parameters of the proposed commercial fusion plant is the international project ITER. [2]. Individual designs of ITER blanket testing modules (BTM) consider LM, Pb-Li, for the most part, as the heat transfer medium. This alloy is proposed to be used as the neutron breeder and heat transfer medium for BTM cooling loops [3].

Experimental studies of different configurations of the LM flow in pipes and channels with different magnetic field orientation and gravity are being made by the joint team of MPEI – JIHT of the Russian Academy of Sciences on mercury test stands [4, 5]. Numerical modeling of the process under study are being made simultaneously [6]. This article is dedicated to the study of hydrodynamics and heat exchange in response to LM buoyancy flow in a coplanar MF in a rectangular channel under the conditions of non-uniform (one-sided) heating. The study is performed to support engineering

solutions related to joint Russian-Indian ITER BTM design having similar flow configuration. This flow configuration measurably affects heat exchange both of a MF and TGC.

## 2. Problem Statement

Figure 1 shows the LM flow pattern under study in mass force fields. Mercury steady flow and heat exchange is considered in the vertical (rectangular) flat channel in the coplanar (*B* magnetic vector is oriented along the wide channel wall $B_x \neq 0$) MF. Aspect ratio in the channel cross-section: *a/b* = 56/17 mm/mm. Channel walls are manufactured from 2.5-mm 12Kh18N10T stainless steel. The flow is buoyant, backward gravity acceleration *g* in the vertical channel with potential independent heating of each wide channel wall under the conditions of measurable opposing thermal gravitational convection affect the flow and heat exchange. Different options of heating the wide channel walls were considered, between double-sided to one-sided with heat flow density $q_c$, as figure 1 (b) shows.

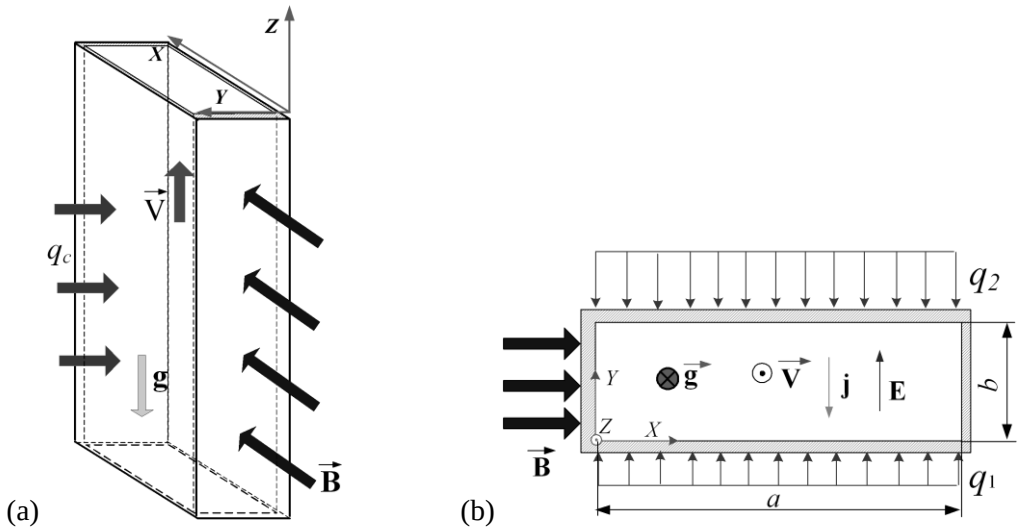


**Figure 1.** The flow pattern under study in the fields of mass forces (a) and in the channel section (b).

Double channel width $d = 2b$ is assumed as the typical size. This scale is the equivalent diameter for the flat channel $d = 4S/P = 2b$.

The rectangular channel inlet has a hydrodynamic stabilization section $Z_0 = z_0/(2b) = 30d$, then, LM enters the heated section with steady heat flow density on both channel sides $q_1$ and $q_2$. The LM section matches the 30*d*-long heating section. The MF diagram has a trapezium shape: the inlet-outlet sections where the MF linearly increases or decreases exerts through 3*d*, and on constant MF section - 24*d*. Farther, $Z_{out} = 5d$ section follows where heating and MF required for pressure computation correction are missing.

Channel walls are assumed to be conductive. Mercury specific resistance is assumed to be equal to $\rho_e = 97.6$ Ohm·m, steel specific resistance $\rho_e = 75$ Ohm·m. Steel conductivity relative to mercury is assumed to be 97.6/75.

## 3. Derivation of Equations

Let us review the steady flow of incompressible medium – LM. The flow and heat exchange may be described with the following vector-type differential equation system [7, 8]:

$$\nabla \cdot \mathbf{V} = 0 \tag{1}$$

$$\rho(\mathbf{V} \cdot \nabla)\mathbf{V} = -\nabla p + \mu \Delta \mathbf{V} + \mathbf{f} \tag{2}$$

$$\rho C_p (\mathbf{V} \cdot \nabla) T = \lambda \Delta T \tag{3}$$

The mass force vector (buoyancy force and electromagnetic force in this task):

$$\mathbf{f} = \rho g \beta (T - T_0) + \mathbf{j} \times \mathbf{B} \tag{4}$$

To compute current density vector j, let us write the Ohm's law as follows:

$$\mathbf{j} = \sigma(\mathbf{E} + \mathbf{V} \times \mathbf{B})\mathbf{j} \tag{5}$$

where **E** – electric field intensity, σ – LM conductivity.

Here: (1) – the continuity equation, the liquid medium conservation law; (2) – the motion equation; momentum conservation law ρ**V**; (3) – the energy equation, the driving medium specific enthalpy conservation law. For this purpose, the following symbols were assumed: ρ – density; $p$ – pressure; μ – dynamic viscosity; $C_p$ – heat capacity of the medium; λ – heat conductivity; β – thermal volume-expansion coefficient; g – free fall acceleration; $T$ – liquid temperature; $T_0$ – pipe inlet temperature. Coordinate differentiation in these equations is shown as operator ∇; divergence of velocity vector **V** – as the dot product ∇·**V**; scalar temperature field gradient– as ∇·$T$; scalar temperature field Laplasian – as Δ$T$, vector velocity field Laplasian– as Δ**V**.

Equations (1) – (3) were reduced to non-dimensional form and for averaged variables were written as:

– the motion equation

$$(\mathbf{V} \cdot \nabla)\mathbf{V} = -\nabla p^* + \frac{1}{\mathrm{Re}}\left(\nabla \cdot \left(1 + \frac{\varepsilon_T}{\nu}\right)\nabla\right)\mathbf{V} + \mathbf{F} \tag{6}$$

– the energy equation

$$(\mathbf{V} \cdot \nabla)\Theta = -\frac{1}{\mathrm{RePr}}\left(\nabla \cdot \left(1 + \frac{\mathrm{Pr}}{\mathrm{Pr}_t}\frac{\varepsilon_T}{\nu}\right)\nabla\right)\Theta \tag{7}$$

The source of mass forces considering the effect from TGC electromagnetic forces:

$$\mathbf{F} = \frac{\mathrm{Gr}_q}{\mathrm{Re}^2}\Theta\mathbf{g}^* + \frac{\mathrm{Ha}^2}{\mathbf{Re}}(\mathbf{j}^* \times \mathbf{B}^*)$$

Here: velocity **V** is related to average velocity $V_0$, $p^*$ – dynamic pressure related to scale $\rho V_0^2$; induction $\mathbf{B}^*$ – to external MF induction $B_0$; current density $\mathbf{j}^*$ – to $\sigma V_0 B_0$; electric field strength $\mathbf{E}^*$ is related to scale $V_0 B_0$; $\varepsilon_T$ – turbulent viscosity coefficient; ν – kinematic viscosity coefficient. The shown non-dimensional description includes the following non-dimensional numbers: $\mathrm{Re} = V_0\, d / \nu$, $\mathrm{Gr}_q = g\ \beta\ q_c\ d^4 / \lambda\ \nu^2$, where $q_c = (q_1 + q_2)/2$ – average density of the heat flow; Pr – Prandtl number; $\mathrm{Ha} = B_0 d(\sigma/\mu)^{0.5}$ – Hartmann number; Pe = Re Pr – Peclet number. Buoyancy forces defined by $\mathrm{Gr}_q/\mathrm{Re}^2$, are a gravity-to-inertia force ratio. Electromagnetic force (the Lorentz force) is defined by $\mathrm{Ha}^2/\mathrm{Re}$, being an electromagnetic-to-inertia force ratio.

Prandtl number $\mathrm{Pr} = (\mu\rho C_p)/\lambda$, turbulent Prandtl number $\mathrm{Pr}_t = \varepsilon_t/\varepsilon_q$; Θ – non-dimensional temperature difference, estimated by the formula $\Theta = (T - T_0)/(q_c d/\lambda)$. In these expressions: $\mathbf{g}^* = \mathbf{g}/g$ – non-dimensional gravity vector; $\varepsilon_q$ – turbulent heat transfer coefficient. Double channel width $d = 2b = 34$ mm is assumed as the length-scale, corresponding to the equivalent diameter of the flat close-clearance channel. Before the working section, there is a hydrodynamic stabilization section of length 30$d$, then follows the heated section with heat flow density on two long channel sides $q_1$ and $q_2$ . The article shows one of the heating options – one-sided ($q_1 = 0$, $q_2 \neq 0$). The 24-long uniform MF section matches the 30$d$-long heated section.

At the channel inlet, the velocity profile was assumed to be unit: $|\mathbf{V}| = 1$. At the channel inlet, a steady flow condition was provided. The heat flow on the wall was defined in the non-dimensional form with expression $q_c^*$ =. $1/\mathrm{Pe}(\partial\Theta/\partial R)_c = -1/\mathrm{Pe}$. Turbulent Prandtl number:.$\mathrm{Pe}_t = 1$

Using the charge conservation equation, the link between electric field strength and electric field potential ($\mathbf{E} = -\nabla\psi$) and Ohm law (7) we will obtain the electric field potential equation:

$$\Delta\psi = \nabla \cdot (\mathbf{V} \times \mathbf{B}) \tag{8}$$

In the process of computations, wall electric conductivity was assumed to be 32 times less than stainless steel conductivity at room temperature. This assumption is based upon the fact that when the experiment was performed, a thin oxide and contamination layer reducing wall conductivity is accumulated on the wall. Direct measurements of the drag coefficient showed that pressure losses

correspond to the MHD-flow in the channel with low-conductivity walls with approximately the same conductivity.

With no MF, let us compute the turbulent transfer coefficients using Reihardt correlations [7]:

$$\frac{\varepsilon_\sigma}{\nu}=0.4\left(y^+-11\text{th}\frac{y^+}{11}\right),\quad y^+\le 50$$
$$\frac{\varepsilon_\sigma}{\nu}=0.133y^+\left(0.5+R_0^2\right)(1+R_0),\quad y^+>50 \tag{9}$$

where $y^+ = \frac{yu_*}{\nu}$, $u_*\sqrt{\frac{\tau_c}{\rho}}$, $y = r_0 - r$, $R_0 = \frac{r}{r_0}$

Finally, we will obtain $y^+ = (1-R)\frac{\mathrm{Re}}{2}\sqrt{\frac{\xi_\infty}{8}}$, where $\xi_\infty = \frac{0.3164}{\mathrm{Re}^{0.25}}$

Although these correlations are obtained for a pipe, they are true for a flat channel being the limit case of the ring channel as well. The validity of this statement is confirmed by the data of test computations. The same model is used in the rectangular channel, where $r$ is measured from the channel axial plane, we assume channel half width - $r_0 = 0.5b$ as $r_0$, measuring $y^+$ coordinate from the closest channel wall side.

In the MF at Ha = 300, 500 and 800, $\varepsilon_T = 0$ was assumed. Since the critical Reinolds number $\mathrm{Re}_{cr,Ha}$ in the coplanar MF may be computed using the correlation $\mathrm{Re}_{cr,Ha}/\mathrm{Ha} = 130$ [8], hence, practically in all flow conditions at $\mathrm{Re} < \mathrm{Re}_{cr,Ha}$ turbulence shall be suppressed in full and $\varepsilon_T = 0$.

The equation system (6–9) was solved as part of the package for numerical modeling of hydrodynamics and heat-mass exchange processes ANES20XE [9].

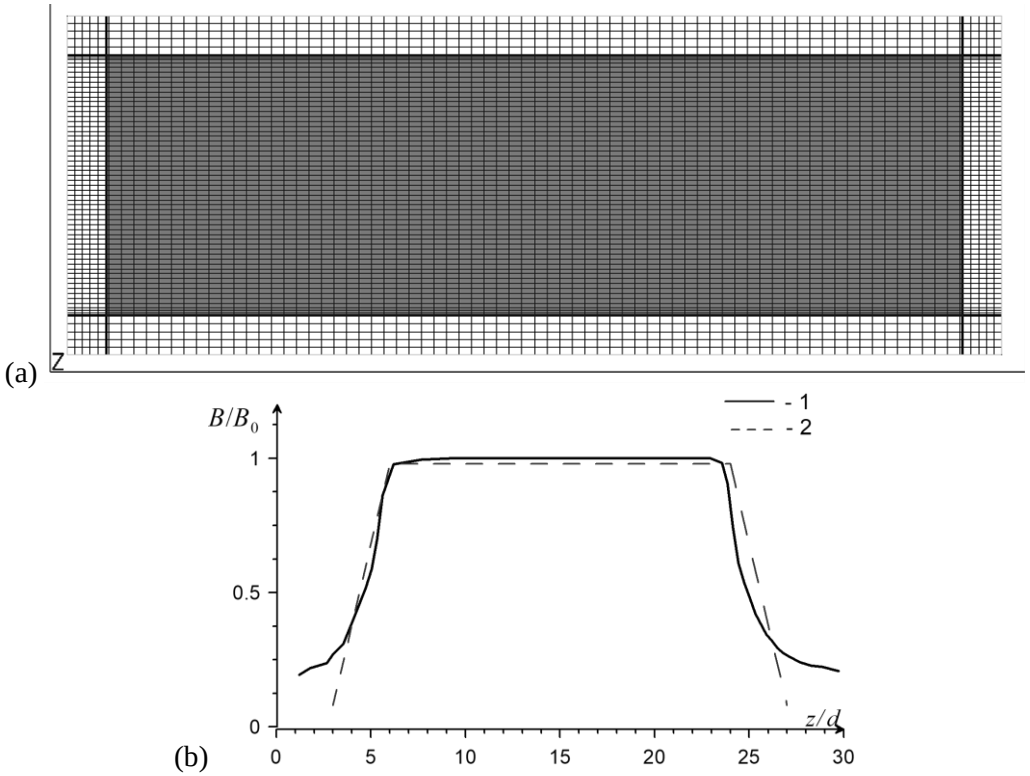


**Figure 2.** Calculated grid in the channel section (a). Plot MF (b) in relation to the heating section: 1) experienced, 2) used in the calculation.

Figure 2 (a) shows number of cells in the channel cross-section is $N_x/N_y$=90/60. Of which 6 cells fall on near-wall (0.01÷0.02)$b$-thick layer getting denser towards the wall. 5 cells fall on the stainless steel $d_w$=(2.5/17)$b$-thick wall.

The computational section in Z-direction includes hydrodynamic stabilization section $Z_0$=10 (60 cells in size), heated section within the MF area $Z_{qB}$=30 (300 cells in size), and outlet section $Z_{add}$=5 (10 cells in size), required to correct the pressure.

The MF plot, used in calculations with a channel of rectangular cross section in the shape of a trapezoid, is shown in figure 2 (b) in comparison with the actual one, measured directly on an experimental stand.

## 4. Numerical Modeling Data

The set of numerical computations related to modeling hydrodynamics and heat exchange in response to the mercury down-flow in the channel provided one of the wide sides (a-long) of the rectangular channel is heated with heat flow density $q_1$=*0* and $q_2$=35000 W/m$^2$ in the coplanar MF with Hartmann numbers Ha=0, 120, 300, 500, 800 in geometry corresponding to the experiments was performed on the mercury MHD-test stand of MPEI – JIHT of the Russian Academy of Sciences [10]. The following data compared with the experimental data obtained in similar conditions are provided. The methodology of experimental studies is detailed in [10, 11].

In this paper, the three-dimensional channel flow, inclusive of the unheated hydrodynamic stabilization section with no magnetic field, heating section matching the uniform coplanar MF area, including the inlet and outlet sections, was numerically simulated. Hence, the averaged variables were obtained on the three-dimensional computational grid: pressure fields, velocity and temperature component, electric field potential component and current density component. To date, at the experimental studies stage, details related to the temperature fields and heat transfer, velocity profiles in the flow section at *Z*=21-distance from the heating start, as well as along the channel length in *Y*-*Z*-section plane with *X*=*x*/b=2.45-coordinate have been obtained [11]. Consequently, data compared exactly in these channel sections are provided below.

In non-isothermal flow, the turbulent stream is additionally affected by buoyancy forces, the value of which is in proportion to the temperature gradient or Gr/Re$^2$. Buoyancy forces are the highest in proximity to the channel walls, oriented upwards and accelerate the buoyant flow within this section. Hence, TGC resists friction forces accelerating the near-wall flow.

When the conductive medium – the liquid metal – flows in the transverse (coplanar) MF due to electromagnetic interaction, flow hydrodynamics strongly varies, the MF suppresses turbulence. The transverse (coplanar) MF causes electric currents in flow cross-section in line with Ohm's law: $\vec{j} = \sigma_e \cdot (\vec{E} + \vec{v} \times \overrightarrow{B})$. Current interaction with the external magnetic field results in the occurrence of a deceleration force, increase in hydraulic resistance and variation in velocity profiles predominantly in the direction of MF induction, the Hartmann effect [6]. All these factors affect heat exchange.

Figure 3 shows the potential distribution of the electric field and the vector field of the electric currents for the Ha = 800 mode. Electric currents interacting with the external magnetic field give rise to the electromagnetic force affecting the velocity profile forms. Currents generated by the magnetic field are practically uniform in the liquid and for the most part are contained in the thin near-wall layer (close to the narrow sides) and channel walls perpendicular to the MF.

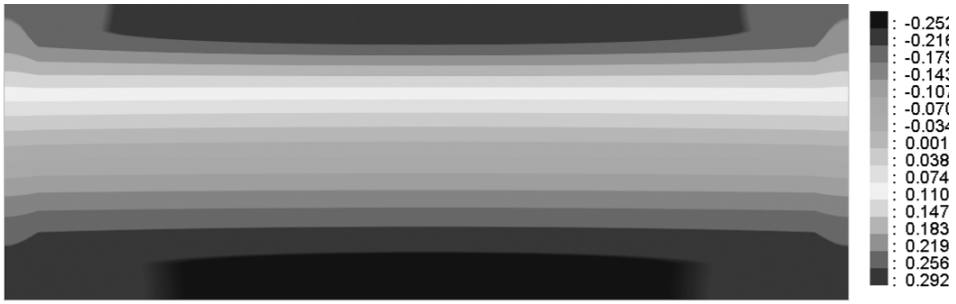


(a)

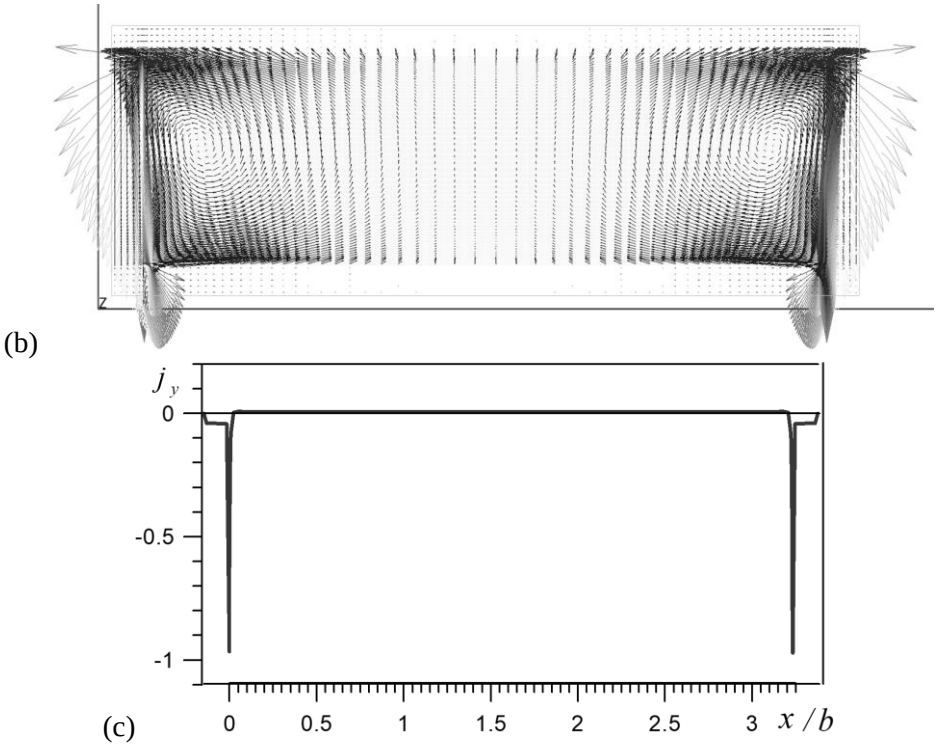


**Figure 3.** Potential (a) and the vector field of electric currents (b) in the cross section of the channel, Re = 30000, Ha = 500. The electric current density $j_y$ (c) in the axial plane along the X axis.

Let us first review flow condition computational data for relatively high Reynolds number Re=50000.

Evidently, in non-isothermal flow the turbulent stream is additionally affected by buoyancy forces, the value of which is in proportion to Grashof's number. In the coplanar MF, one may observe flattening of velocity profiles in the *X*-direction in line with the above Hartmann effect.

Figure 4 shows longitudinal velocity component profiles with no MF and in the coplanar MF in two vertical planes in $X=x/b$ and $Y=y/b$ directions running through the channel center.

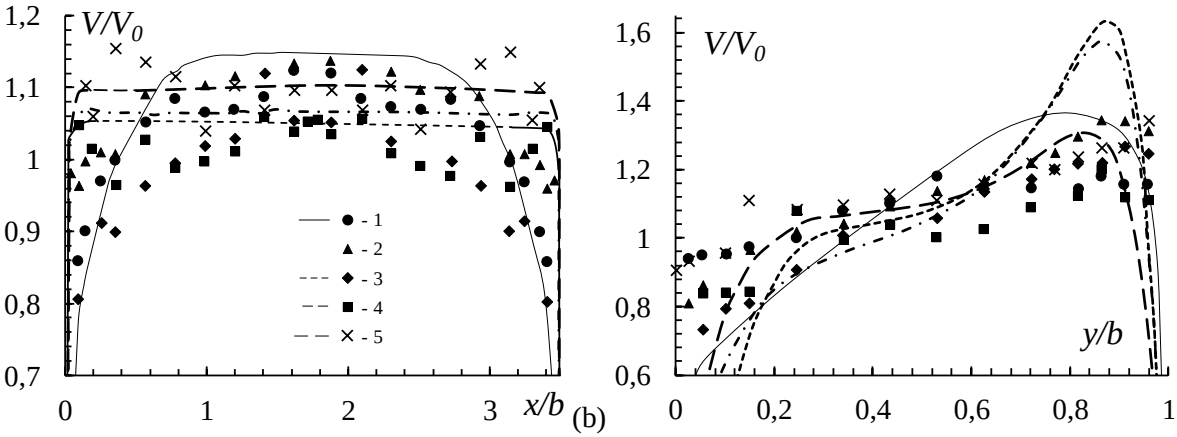


**Figure 4.** Profiles of dimensionless velocity in the cross section of the channel along the X (a) and Y (b) axis, $q_1/q_2$= 0/35 kW/m$^2$, Re =20000: 1) Ha=0; 2) Ha= 120; 3) Ha= 300; 4) Ha=500.

The absence of MF design profiles is highlighted with red lines, experimental data – with symbols. Experimental points were obtained with the correlation thermocouple sensor [11]. The effect from buoyancy forces in these conditions with high Reynolds numbers is relatively low, although measurable based upon *Y*-axis profiles. In general, a reasonably good fit of the calculated data to the

experimental ones is observed with due account for measurement error and low method accuracy in proximity to the wall.

Non-dimensional temperature is defined by value $\Theta = \frac{\lambda}{d}\frac{T-T_0}{q_c}$, where $T$ – the local temperature, heat flow density is defined as the average for two pipe sides $q_c$=0.5·($q_1$+$q_2$). Such definition $q_c$ is selected for reasons of similarity for comparison of different heating options ($q_1$=$q_2$ и $q_1$≠$q_2$).

Regarding heat transfer, as already mentioned, it is more suitable to apply exactly the non-dimensional wall temperature, since the local heat transfer coefficient (Nusselt's number) formally equal to Nu=1/$\Theta_c$ may have no sense here. Strong non-uniformity in wall temperature distribution in the direction of the channel cross-sections increasing in the magnetic field is detected in the flow and heating configuration under study. This fact is of value under actual heat exchange conditions in the fusion reactor since it causes measurable thermal stresses requiring consideration in the strength engineering calculations.

Further, the figure shows data obtained in the *Y-Z* section with *X*=2.5 coordinate (in a quarter of channel width) along the length with the longitudinal rack-type probe. Non-dimensional temperature distribution along the channel length (figure 5) obtained for two generators on the heated and unheated channel sides (black and light symbols) are the most interesting. The left curve of figure 5 (a) shows that for Re=20000 the temperature of the heated (unheated) wall starting from the inlet increases (decreases) steadily to some value of the non-dimensional axial coordinate, approximately *z/d*=15, and reaches the fixed level. The nature of temperature variation in the *z* direction allows a judgement on the length of the initial thermal section. Under these conditions, it is approximately 15 calibers. The left curve of figure 5 (b) shows that for Re=50000 no stabilization is observed - the entire heating section is the initial section.

Coincidence of the calculated curves and experimental points here is not bad, both in the magnetic field for different Hartmann numbers and with no field. The left curve of figure 5 (a) shows that for Re=20000, the experimental point and calculated curves start to deviate at the final heating section in the MF. This is related to TGC effects, the relative influence of which increases as the Reynolds number decreases in accordance with the Gr/$Re^2$ increase. An even stronger difference is observed under conditions with lower Reynolds numbers Re=10000–12000. The buoyancy forces accelerating the flow in proximity to the heated wall increase velocity gradients causing flow instability in the MF and occurrence of turbulent vortexes and generation of large-scale vortices with axes oriented along MF induction. Since these vortices interact weakly with the coplanar MF, the effect develops steadily. Secondary vortices caused by TGC in MF laminar flow additionally mix the liquid, consequently, the wall temperature decreases.

The described effect is more evident in the double-sided heating options. Turbulent pulses were not observed even in the strongest MF under some suppression conditions, and intensive low-frequency bursts associated with high-frequency temperature variations were detected. Similar low-frequency high-intensity temperature fluctuations were detected by us in the *down*-flow during previously performed studies [11].

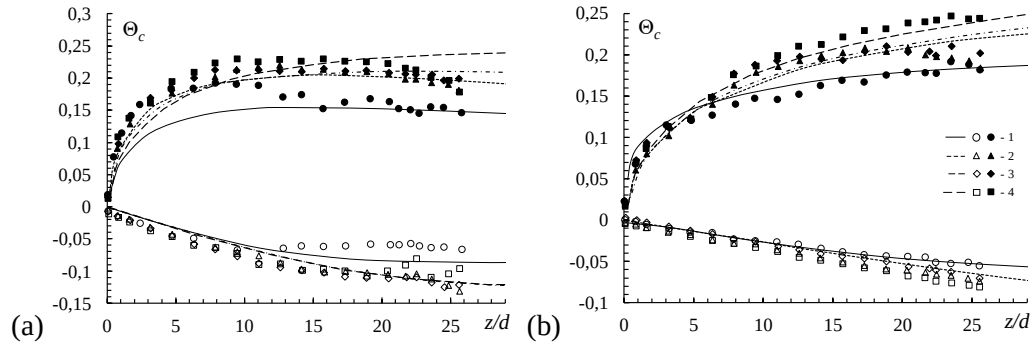


**Figure 5.** The distribution of the dimensionless wall temperature $\Theta_c$ along the length of the channel on the unheated (light symbols) and on the heated sides (filled symbols), Re = 20000 (a) and Re = 50000 (b): 1) Ha=0; 2) Ha=300; 3) Ha=500; 4) Ha=800.

It is clear, that the described model does not consider all TGC effects specific for magnetic channel LM-flow hydrodynamics. Hence, the calculated model requires subsequent development and progress is being made.

## 5. Conclusion

Hydrodynamics and heat exchange of the configuration of LM buoyant flow in the rectangular channel with approximately 3/1 aspect ratio in the coplanar MF under the condition of double-sided heating of wide channel sides was studied on the mercury test stand of JIHT of the Russian Academy of Sciences. The authors proposed a model for numerical modeling of the flow parameters under study under experimental conditions.

Averaged velocity, temperature, through-wall temperature distribution profiles are shown in one-sided channel heating conditions. Computational data obtained with probe techniques both in the cross-section and along MHD-channel length are compared with experimental data within the range of operating conditions.

Strong non-uniformity in wall temperature distribution along the channel section perimeter increasing in the coplanar magnetic field is observed in the configuration of LM buoyant flow in the rectangular channel in the process of one-sided heating.

In general, the experiment data coincide well with the computational data, which indicates the satisfactory capability of the calculation model under experimental conditions and possible application of real heat exchangers in fusion reactor design.

MHD-effects related to generation of non-isotropic turbulence and occurrence of low-frequency high-amplitude temperature fluctuations are observed under some flow conditions with relatively high $Gr/Re^2$ values. These fluctuations occur due to the development of secondary large-scale flow structures caused by the joint effect upon mass force flow, both electromagnetic and gravitational. The proposed calculation model does not consider these effects and under appropriate heat exchange conditions, the experimental data coincide with the computational data less well. Subsequent development of the calculation model is required.

## References

[1] Velikhov E P, Kovalchuk M V and Azizov E A 2014 *PAS&T*.TF **4** 5
[2] ITER Organization. Annual report 2013
[3] Salavy J F, Kim Y, Kirillov I and Morley N B 2008 Fusion Engineering and Design **83** 850
[4] Belyaev I A, Genin L G, Listratov Ya I and Sviridov V G 2013 Magnetohydrodynamics **49** 177
[5] Belyaev I A, Sviridov V G and Razuvanov N G 2015 High Temperatures **5** pp 1-9
[6] Zikanov O, Listratov Ya I and Sviridov V G 2013 Journal of Fluid Mechanics **720** 486
[7] Genin L G and Sviridov V G 2001 *Hydrodynamics and heat transfer of MHD flows in channels* (Moscow: Moscow Power Engineering Institute)
[8] Branover G G and Tsinober A B 1970 *Magnetic hydrodynamics of incompressible medium* (Moscow: Science Press)
[9] Yankov G G, Artyomov V I and Karpov V E 2000 Thermal Engineering **7** 52
[10] Genin L G, Listratov Ya I, Sviridov V G and Razuvanov N G 2003 *PAS&T*.TF **4** 35
[11] Poddubny I I and Razuvanov N G 2016 Thermal Engineering **2** 13

## Acknowledgments

Work is supported by RSF project № 14-50-00124.

Experiments are performed on the RF UNU “Mercury MHD stand”.

The calculations are carried out in the Joint Supercomputer Center of the Russian Academy of Sciences.